Degree-of-linear-polarization-based Color Constancy

Taishi Ono   Yuhi Kondo   Legong Sun   Teppei Kurita

Yusuke Moriuchi

Sony Group Corporation, Tokyo, Japan

{Taishi.Ono,Yuhi.Kondo,Legong.Sun,Teppei.Kurita,Yusuke.Moriuchi}@sony.com
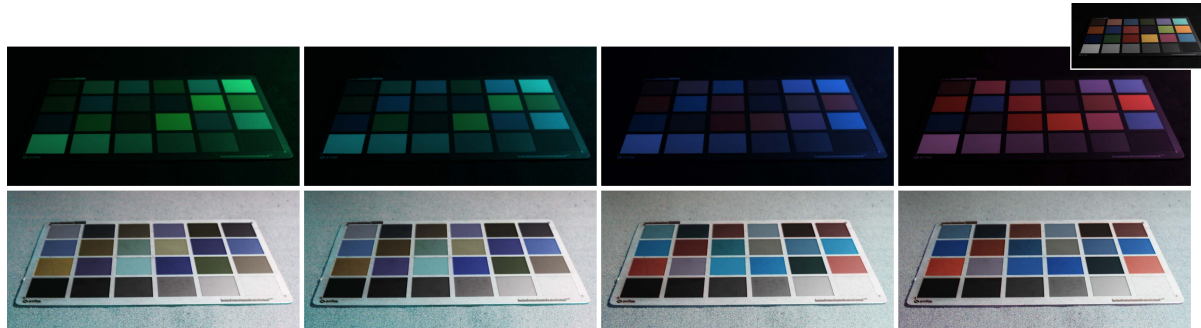
Figure 1. **Degree of linear polarization (DoLP) of achromatic pixels are always achromatic regardless of the illumination colors.**
Raw-RGB images (top) and their DoLP values of RGB (bottom). Achromatic patches located in the bottom rows have always achromatic
DoLP values.

Abstract

Color constancy is an essential function in digital photography and a fundamental process for many computer vision applications. Accordingly, many methods have been proposed, and some recent ones have used deep neural networks to handle more complex scenarios. However, both the traditional and latest methods still impose strict assumptions on their target scenes in explicit or implicit ways. This paper shows that the degree of linear polarization dramatically solves the color constancy problem because it allows us to find achromatic pixels stably. Because we only rely on the physics-based polarization model, we significantly reduce the assumptions compared to existing methods. Furthermore, we captured a wide variety of scenes with ground-truth illuminations for evaluation, and the proposed approach achieved state-of-the-art performance with a low computational cost. Additionally, the proposed method can estimate illumination colors from chromatic pixels and manage multi-illumination scenes. Lastly, the evaluation scenes and codes are publicly available to encourage more development in this field.

1. Introduction

When a light source illuminates an object, the observed color is determined by the reflectance of the object and the illumination color. The goal of color constancy is to separate the illumination color from the observation and obtain an image equivalent to one captured under achromatic illumination. Because human vision inherently has this ability [6], color constancy is vital for digital photography to capture suitable images for human preferences. Additionally, color constancy is critical for various computer vision applications [5, 23, 57], including methods using deep neural network (DNN) [2]. However, color constancy is still a challenging problem because separating the material reflectance and illumination color from observation is fundamentally ill-posed.

Some studies have introduced statistical knowledge about objects or illuminations in scenes to overcome the difficulty. Gray-world [12] and its extensions [17, 51] exploit the assumption that the average value of objects' reflectance in a scene becomes achromatic. White-patch methods [20, 35] assume that scenes include perfect reflection and regard the area as the representation of the illumination color. However, natural scenes frequently violate these statistical expectations, which significantly degrades the quality of the results.

Regarding data-driven algorithms, several illumination-estimation models have been developed using training data sets [11, 21, 23, 31]. More recently, methods that exploit DNNs have been proposed and have achieved higher performance [30,41,47]. Furthermore, several approaches have

introduced new learning frameworks to handle images captured by unknown cameras [1,29,39,54,58]. However, these learning-based methods are still highly dependent on the quality of the training data.

Speaking of polarization, it could help solve the color constancy problem because diffuse (representing material color) and specular (representing illumination color) polarization behave differently [53]. For instance, several studies have estimated illumination colors by assuming that only the specular reflection is polarized [18, 45], meaning that polarization amplitude directly represents the illumination color. However, because diffuse reflection also affects polarization [9, 33], this assumption incorrectly estimates illumination colors, especially when diffuse reflection dominates the scene.

In this paper, we show that degree of linear polarization (DoLP) significantly contributes to solving the color constancy problem because it allows us to find achromatic pixels stably. Our main idea is quite simple: *the DoLP values of achromatic pixels are also achromatic regardless of the illumination colors.* Figure 1 shows several color charts captured under different illuminations. Focusing on the achromatic squares located on the bottom row of the color chart, we notice that their DoLP values are always achromatic despite the drastic change of illumination colors. In summary, our contributions are as follows:

- We propose the first approach to indicate the dramatic contribution of DoLP to solving the color constancy problem.

- Our method achieved state-of-the-art performance at a low computational cost on our new evaluation data, which include a wide variety of illuminations.

- The proposed approach is robust because it is independent of statistical knowledge about reflectance or illuminations, free from any optimization or training processes, and accurately considering diffuse polarization.

- We widely analyzed how to estimate illuminations from chromatic pixels and examined a solution for multi-illumination scenes.

- Our codes and the created evaluation data are publicly available to encourage more advancement in this field.

2. Related work

As described in Sec. 1, the color constancy problem is ill-posed because many pairs of material reflectance and illumination color can generate the same results. Many algorithms have been proposed to address this ambiguity,

and the classical group is static approaches. The Gray-world algorithm assumes that the average reflectance in a scene is achromatic [12]. Several methods have extended this assumption by relying on areas having more textures [13,26,51]. Two-stage algorithms have also been proposed, searching for achromatic pixels in a scene and executing Gray-world on the labeled pixels [16, 37, 42, 55]. On the other hand, the White-patch algorithm [19, 20, 35] assumes that a perfect reflection causes the maximum intensity in a scene, thus representing the illumination color. Additionally, the combination of the Gray-world and White-patch has been examined [17, 25]. Furthermore, several studies have introduced physics-based reflectance models [28, 49, 50]. The abovementioned static approaches often work well, and their computational cost is generally low, but natural scenes frequently violate their statistical assumptions.

Another large category of color constancy algorithms is learning-based approaches, which are becoming more popular. Some studies have applied support vector regression [21, 52], kernel regression [4] or ridge regression [3]. More recently, a few methods have defined the color constancy problem as a classification problem in a unique color space [10, 11]. Furthermore, many studies have exploited DNNs to deal with more complicated scenes [30, 41, 47]. Because these methods do not perform well for unknown cameras, other methods have addressed the issue by using a few additional images when estimating illuminations [1], introducing a re-weighting module [54], generating several candidate images and their likelihood [29], and exploiting contrastive learning to acquire more general feature [39]. These data-driven approaches perform better, especially for complex scenes, but their results heavily depend on training data distribution, and acquiring images with ground-truth illumination colors is usually laborious.

For polarization, it has been proven that the polarization of reflected light is related to the surface normal of the reflection point. Therefore, polarization has long been used for surface normal estimation [7, 43, 44, 48, 53]. Additionally, because polarization behaves differently depending on diffuse or specular reflection, several studies have exploited polarization to separate reflected and transmitted light occurring at glass surfaces [36, 38, 40]. Furthermore, other methods have applied polarization analysis for estimating illumination colors by assuming that only specular reflection is polarized [18, 45]. Based on this assumption, polarization amplitude directly represents the illumination color, but this is easily violated because diffuse reflection is also polarized. Therefore, more accurate models that consider both diffuse and specular polarization have recently been introduced [9, 33]. Additionally, the development of the polarization camera [56] has made it much easier to capture polarization information. On the whole, polarization has

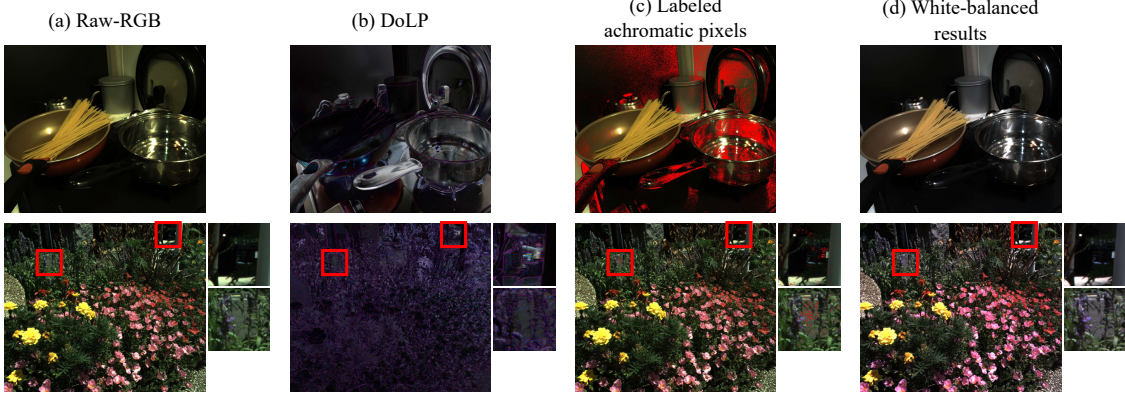| (a) Raw-RGB | (b) DoLP | (c) Labeled achromatic pixels | (d) White-balanced results |

Figure 2. **Concept of our DoLP-based color constancy.** The input is raw-RGB (a) and DoLP (b) images. First, we search achromatic pixels based on the chromaticity of DoLPs (c) and then acquire white-balanced results (d). Note that we also use chromatic pixels and introduce weighting schemes to acquire final results, explained in Sec. 3.4 and Sec. 3.5, respectively.

been widely studied, but no color constancy method with an accurate polarization model that considers both diffuse and specular reflection has been proposed.

3. Method

3.1. Problem definition

When an RGB camera is used to capture light reflected by an object, the observed intensity i_j of a pixel can be described as

$$i_j = \int_\omega c_j(\lambda) r(\lambda) l(\lambda) d\lambda, \tag{1}$$

where λ denotes the wavelength, ω is the range of the visible spectrum, and c_j is the camera sensitivity function corresponding to the sensor's color channel $j \in \{R, G, B\}$. r represents the reflectance of the object, and l is the spectrum of the incident light.

Besides, under the assumption of narrow spectral response, the function Eq. (1) can be approximately regarded as the product of the surface reflectance $r_j \in \{r_R, r_G, r_B\}$ and the illumination observed by the camera $l_j \in \{l_R, l_G, l_B\}$. Under this assumption, Eq. (1) is revised as

$$i_j = r_j l_j. \tag{2}$$

Given the observation i_j, the goal of color constancy is to estimate l_j and to obtain a white-balanced image $\boldsymbol{i}_{WB} = (i_R \cdot l_G/l_R, i_G, i_B \cdot l_G/l_B)$.

3.2. Polarization model

When a surface reflects light, the reflection changes the polarization of the light. This process is described by multiplying a Mueller matrix $M \in \mathbb{R}^{3\times3}$ and a Stokes vector $\boldsymbol{s} \in \mathbb{R}^3$ as $M\boldsymbol{s}$. Note that we do not consider the fourth dimension representing circular polarization in this paper. Besides, when observing a Stokes vector $\boldsymbol{s} = (s_0, s_1, s_2)^T$,

its DoLP is computed as $\sqrt{s_1^2 + s_2^2}/s_0$, and angle of linear polarization (AoLP) is $\frac{1}{2}\tan^{-1}(s_2/s_1)$.

Based on a dichromatic reflection model [46], reflectance r in Eq. (1) is divided into specular reflectance r_s and diffuse reflectance r_d. Furthermore, the specular and diffuse reflections have their own Mueller matrices M_s and M_d [9,33], respectively. Given that the specular component is independent of wavelength, Eq. (1) is updated as

$$\begin{pmatrix} i_{0j} \\ i_{1j} \\ i_{2j} \end{pmatrix} = \left[r_s M_s \int_\omega c_j(\lambda) l(\lambda) d\lambda + \right.$$
$$\left. M_d \int_\omega c_j(\lambda) r_d(\lambda) l(\lambda) d\lambda \right] \begin{pmatrix} l_0 \\ l_1 \\ l_2 \end{pmatrix}, \tag{3}$$

where $(l_0, l_1, l_2)^T$ and $(i_{0j}, i_{1j}, i_{2j})^T$ denote the Stokes vector of the incident light and observation, respectively. Note that we do not assume Muller matrices are dependent on wavelength, which is an assumption frequently used in polarization-related studies [48]. Additionally, we expect the Stokes vector of the incident illumination to be independent of the wavelength. Given that many polarization-based methods assume that illuminations are unpolarized ($l_1 = l_2 = 0$) [8,15,32], this assumption is rarely violated, except under multi-reflection. Besides, this function also assumes that a pixel is predominantly illuminated by one light source. These limitations are discussed in Sec. 6.

3.3. DoLP-based color constancy

When a pixel is achromatic, its diffuse reflection r_d is free from wavelength λ. Thus, Eq. (3) becomes

$$\begin{pmatrix} i_{0j} \\ i_{1j} \\ i_{2j} \end{pmatrix} = \int_\omega c_j(\lambda) l(\lambda) d\lambda \left[r_s M_s + r_d M_d \right] \begin{pmatrix} l_0 \\ l_1 \\ l_2 \end{pmatrix}. \tag{4}$$

When we express the computed result of the integral part in Eq. (4) as K_j and denote the remaining part $[r_s M_s + r_d M_d](l_0, l_1, l_2)^T$ as $(s_0', s_1', s_2')^T$, Eq. (4) is revised as

$$\begin{pmatrix} i_{0j} \\ i_{1j} \\ i_{2j} \end{pmatrix} = K_j \begin{pmatrix} s_0' \\ s_1' \\ s_2' \end{pmatrix}. \quad (5)$$

Therefore, the $DoLP_j$ of the observed result becomes

$$\begin{aligned} DoLP_j &= \frac{\sqrt{K_j^2 s_1'^2 + K_j^2 s_2'^2}}{K_j s_0'} \\ &= \frac{\sqrt{s_1'^2 + s_2'^2}}{s_0'}. \end{aligned} \quad (6)$$

It means that when a pixel is achromatic, its $DoLP_R, DoLP_G, DoLP_B$ become the same regardless of the camera sensitivity function $c_j(\lambda)$ and illumination color $l(\lambda)$. Note that this theory explicitly considers the diffuse polarization M_d, and we discuss the benefit in Sec. 5.

Figure 1 shows several raw-RGB images captured under different illuminations (top) and the corresponding DoLP images (bottom). When focusing on the achromatic pixels located on the bottom row of the color chart, it can be seen that the DoLP values of these pixels are achromatic despite the drastic change of illumination colors.

The basic concept of the DoLP-based color constancy is shown in Fig. 2. Firstly, we search achromatic pixels based on the chromaticity of DoLP values. Secondly, we compute illumination colors by considering the RGB colors in these pixels to be the same as the illumination colors ($i_j = l_j$). Note that we use also chromatic pixels and introduce weighting schemes to acquire final results, explained in Sec. 3.4 and Sec. 3.5, respectively.

3.4. Chromatic pixels

For chromatic pixels, we exploit the knowledge that a white-balanced color of a pixel becomes the opposite against its DoLP color. We introduce two expectations: the specular and diffuse polarization cancel out each other because they have different AoLPs, and the specular DoLP is larger than the diffuse one. Therefore, the DoLP is approximately equal to subtracting the diffuse reflection $r_d(\lambda)$ from the specular one r_s, while the white-balanced color equals the sum of $r_d(\lambda)$ and r_s. Denoting RGB values of DoLP as $d_{R,G,B}$, their average as $\bar{d}$, white-balanced result as $\boldsymbol{i}_{WB} = (k_R i_R, i_G, k_B i_B)$, and its average as $\bar{i}$, this relation is expressed as

$$-\frac{k_R i_R - \bar{i}, i_G - \bar{i}, k_B i_B - \bar{i}}{\sqrt{(k_R i_R - \bar{i})^2 + (i_G - \bar{i})^2 + (k_B i_B - \bar{i})^2}} = \frac{d_R - \bar{d}, d_G - \bar{d}, d_B - \bar{d}}{\sqrt{(d_R - \bar{d})^2 + (d_G - \bar{d})^2 + (d_B - \bar{d})^2}}. \quad (7)$$
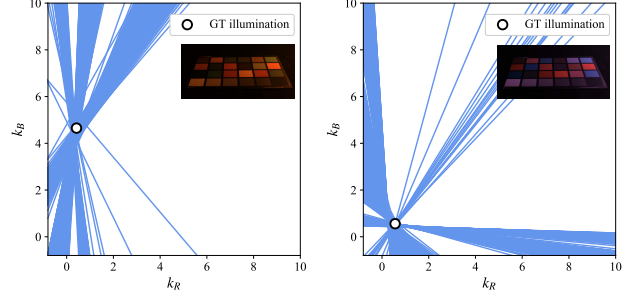

Figure 3. For chromatic pixels, intersection points of the simultaneous equations represent the illumination colors. Equation (8) and ground-truth illuminations plotted in a k_R-k_B space under two different illuminations.

Note that $\boldsymbol{i}_{WB}$ and DoLP are subtracted by their averages and normalized to align their domain differences. By transforming Eq. (7), we obtain the following equation:

$$(d_R - d_B)i_G + (d_B - d_G)i_R k_R + (d_G - d_R)i_B k_B = 0. \quad (8)$$

After observing two or more pixels, we can estimate the illumination color by solving these simultaneous equations.

Figure 3 shows the simultaneous equation Eq. (8) and ground-truth illuminations plotted in a k_R-k_B space under two illuminations. We used chromatic pixels of the color charts to plot this figure. Comparing the intersections of the lines to the ground-truth illuminations, it can be seen that the intersections represent the illumination colors.

3.5. Weighting scheme

We introduce weighting schemes to handle the contribution of each pixel.

Differences between RGB values of DoLP: The candidate achromatic pixels are more reliable when the RGB differences of the DoLP values are smaller. When defining $|DoLP_R - DoLP_G| / \overline{DoLP_{R,G,B}}$ as x and $|DoLP_B - DoLP_G| / \overline{DoLP_{R,G,B}}$ as y, the reliability of achromatic pixels w_{ach}^{dolp} is expressed as

$$w_{ach}^{dolp} = \left\{ 1 - \frac{1}{1 + e^{-a(x-b)}} \right\} \times \left\{ 1 - \frac{1}{1 + e^{-a(y-b)}} \right\}. \quad (9)$$

Figure 4 shows the computed reliability w_{ach}^{dolp} with $a = 50, b = 0.08$. Pixels with higher reliability are plotted as brighter. From this image, we know that the achromatic pixels are accurately computed as more reliable.

Conversely, the candidate chromatic pixels are more reliable when the RGB differences of the DoLP values are larger. We compute w_{ch}^{dolp} as

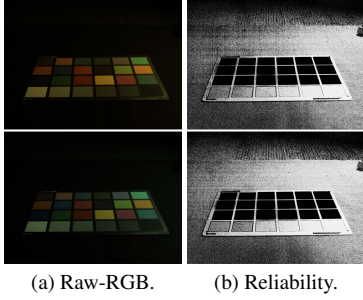$$w_{ch}^{dolp} = \frac{1}{1 + e^{-a(x-b)}} \times \frac{1}{1 + e^{-a(y-b)}}. \quad (10)$$

(a) Raw-RGB. (b) Reliability.

Figure 4. The weight w_{ach}^{dolp} accurately regards achromatic pixels. Raw-RGB images (a) and computed reliability using Eq. (9) with $a = 50, b = 0.08$ (b). Brighter pixels represent higher reliability.

Differences between RGB values of AoLP: We also rely on the AoLP chromaticity to consider ambient illuminations. Because they come from every direction and become unpolarized, when a scene includes the ambient illuminations, Eq. (5) becomes

$$\begin{pmatrix} i_{0j} \\ i_{1j} \\ i_{2j} \end{pmatrix} = \begin{pmatrix} K_j s_0' + l_j^{amb} \\ K_j s_1' \\ K_j s_2' \end{pmatrix}, \qquad (11)$$

where l_j^{amb} denotes the ambient illumination. Because AoLP is free from the first component, it is still achromatic. We use the same function as Eq. (9) for the reliability w_{ach}^{aolp}, where x and y represent $|AoLP_R - AoLP_G|$ and $|AoLP_B - AoLP_G|$, respectively. Regarding the inherent ambiguity of AoLP, see supplementary materials.

DoLP values: Because pixels with small DoLP are highly susceptible to noises, we reduce the contribution from these pixels. When defining an average value of $DoLP_{R,G,B}$ as x, we use the following function:

$$w_{dolp} = \frac{1}{1 + e^{-a(x-b)}}. \qquad (12)$$

AoLP differences for excluding edges: Bayer-RGB sensors assign false colors to the edges, which significantly affects chromatic pixels. Because AoLP differences between RGB channels are typically small except for the edges, we compute w_{ch}^{aolp} to remove these pixels using the same function as Eq. (9). Figure 5 shows a captured image (Fig. 5a), its DoLP (Fig. 5b), and a weighted DoLP (Fig. 5c). Comparing Fig. 5b with Fig. 5c, we see that false DoLP colors along the edges were decreased.

After we calculate all the weights of achromatic pixels $w_{ach}^{dolp} w_{ach}^{aolp} w_{dolp}$ and chromatic pixels $w_{ch}^{dolp} w_{ch}^{aolp} w_{dolp}$ for every pixel in the image, we acquire two illuminations l_j^{ach} and l_j^{ch} by calculating the weighted average of achromatic
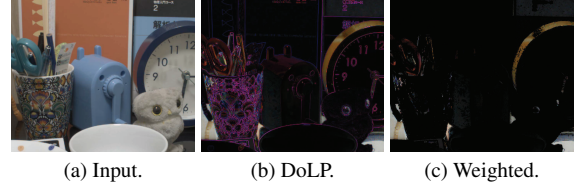

(a) Input. (b) DoLP. (c) Weighted.

Figure 5. The weight w_{ch}^{aolp} precisely removes the edges. Input (a), Corresponding DoLP (b), and DoLP multiplied by w_{ch}^{aolp} (c).
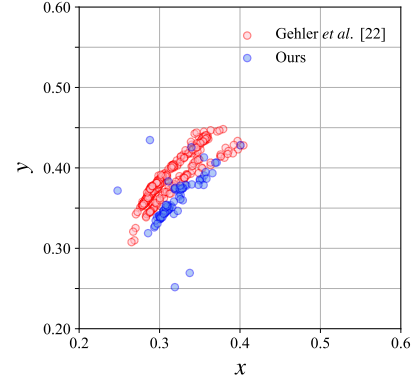

Figure 6. Illumination color comparison between our data and Gehler *et al.* [22]. Illumination colors are mapped to xy chromaticity space.

and chromatic pixels. Lastly, the estimated illumination is the blend of the two illuminations $\alpha l_j^{ach} + (1 - \alpha) l_j^{ch}$.

4. Experiment

Data for evaluation: We used two cameras to capture the evaluation data. The first camera was an FLIR BFS-U3-51S5PC-C implemented with a Sony IMX250MYR color polarization sensor. Each pixel has one of four wire grid polarizer angles ($0°$, $45°$, $90°$, $135°$), so it captures polarization images in a single shot. After capturing, we applied a polarization-demosaicking method [34] to the raw images to obtain four polarization images (i_j^0, i_j^{45}, i_j^{90}, i_j^{135}). The second camera was a Grasshopper3 GS3-U3-41C6C implemented with a CMOSIS CMV4000 color sensor. We located a linear polarizer in front of the camera and captured four polarization images by manually rotating the polarizer. We acquired the observed Stokes vector by calculating

$$\begin{pmatrix} i_{0j} \\ i_{1j} \\ i_{2j} \end{pmatrix} = \begin{pmatrix} (i_j^0 + i_j^{45} + i_j^{90} + i_j^{135})/2 \\ i_j^0 - i_j^{90} \\ i_j^{45} - i_j^{135} \end{pmatrix}. \qquad (13)$$

We captured a total of 82 images using these two cameras. These images included several weather conditions for 27 outdoor scenes and various illumination colors for 55 indoor scenes. For computing the ground-truth illumina-

Method	Mean	Med.	Tri.	Best25%	Worst25%
White-patch [35]	5.38	3.69	4.12	0.99	12.51
Gray-world [12]	5.28	3.94	4.19	1.42	11.68
Shad. gray [17]	9.13	8.20	8.30	2.66	17.43
Gray-edge [51]	8.65	7.37	7.37	2.76	16.90
Weighted-GE [27]	9.16	8.24	8.27	2.83	17.42
Chen *et al.* [14]	5.62	4.05	4.18	1.29	12.88
Qian *et al.* [42]	4.88	2.61	3.03	0.89	13.00
FFCC [11]	7.49	5.17	5.37	1.29	17.93
FC4 [30]	4.21	3.39	3.47	1.65	8.53
C4 [58]	**3.55**	**2.31**	2.73	0.96	**8.01**
C5 [1]	4.83	3.67	3.80	0.99	11.52
Ours	3.82	2.44	**2.65**	**0.60**	9.73

Table 1. Angular errors for all 82 scenes.

Method	Mean	Med.	Tri.	Best25%	Worst25%
White-patch [35]	5.07	3.44	3.94	0.96	11.81
Gray-world [12]	5.41	4.29	4.63	1.44	11.44
Shad. gray [17]	9.20	8.30	8.36	2.49	17.77
Gray-edge [51]	8.76	7.44	7.41	2.65	17.27
Weighted-GE [27]	9.23	8.33	8.31	2.69	17.75
Chen *et al.* [14]	5.43	3.95	4.08	1.24	12.49
Qian *et al.* [42]	4.38	2.55	2.89	0.86	11.43
FFCC [11]	7.38	5.09	5.26	1.23	18.07
FC4 [30]	4.08	3.34	3.38	1.63	8.27
C4 [58]	3.43	**2.25**	2.66	0.93	7.80
C5 [1]	4.67	3.23	3.35	0.96	11.37
Ours	**3.21**	2.29	**2.46**	**0.57**	**7.57**

Table 2. Angular errors for 79 images not including blue skies.

tion colors, each image was paired with the same scene including a color chart, with which we used the third-darkest patch to acquire the ground-truth illuminations. In Fig. 6, we compared the illumination color distribution of our data with Gehler *et al.* [22]. The figure tells us that our data contain broad illumination colors. Note that our data included a few high-saturated illuminations represented by several outliers. For more details, see supplementary materials.

Parameters for weights: Parameters for each weight described in Sec. 3.5 were $a = 50, b = 0.08$ for w_{ach}^{dolp}, $a = 50, b = 1$ for w_{ach}^{aolp}, $a = 50, b = 0.15$ for w_{dolp}, $a = 50, b = 0.2$ for w_{ch}^{dolp}, $a = 50, b = 10$ for w_{ch}^{aolp}, and $\alpha = 0.95$. We manually fixed these parameters by using scenes including the color chart. Note that we used the same parameters for all the data.

Evaluation metrics: To evaluate the errors between the ground-truth l and estimated illuminations $\hat{l}$, we computed the angular error $arccos(\frac{l \cdot \hat{l}}{\|l\| \|\hat{l}\|})$ according to the existing color constancy methods. For a broad evaluation, we reported several metrics about the angular error: mean, median, tri-mean of all the errors, mean of the lowest 25% of errors , and mean of the highest 25% of errors.

5. Results

Comparison with existing methods: We compared our results with both static and learning-based methods. For the static methods, we chose White-patch [35], Gray-world [12], Shades of gray [17], Gray-edge [51], Weighted gray-edge [27], Chen *et al.* [14], and Qian *et al.* [42]. For the learning-based studies, we used FFCC [11], FC4 [30], C4 [58], and C5 [1]. We selected these methods based on their reproducibility. We used MATLAB's built-in functions for White-patch, Gray-world, and Chen *et al.*, and used imple-

mentations available from Gijsenij *et al.* [24] for Shades of gray, Gray-edge, and Weighted gray-edge. For the learning-based methods, we did not train or fine-tune the models using our evaluation data and used parameters provided by the authors.

Table 1 lists the calculated errors for all 82 scenes. For the mean values of all errors, the proposed method performed second-best. Regarding the other metrics, ours was the best for the tri-mean and the mean of the highest 25% errors but third-best for the lowest 25% errors. This is because our method performed poorly when scenes included blue skies, as shown in Fig. 8. As shown in Fig. 8a, because the DoLP values of blue skies are achromatic and are typically not the main light source, our method failed to predict the illumination colors (Fig. 8c), which is discussed in Sec. 6. Therefore, to evaluate our performance without the issue, we excluded three scenes that were dominated by the blue skies. Table 2 lists the results for the 79 images. From this table, it can be seen that we performed best of all methods in terms of mean error, tri-mean, mean of the highest and the lowest 25% errors.

Additionally, we qualitatively compared our results with Gray-world, C4 [58], and C5 [1]. Figure 7 shows seven scenes including several illumination conditions for outdoor and indoor scenes. Because we estimated illumination colors based on the physics-based model, our method performed better especially when color distributions of scenes were biased or scenes were illuminated by a highly saturated illumination.

Advantage of considering diffuse polarization: We examined several scenes dominated by diffuse polarization to demonstrate our theoretical contribution compared to the assumption that disregards the diffuse component. The introduced polarization model of Eq. (3) tells us when the diffuse component becomes larger, the polarization ampli-
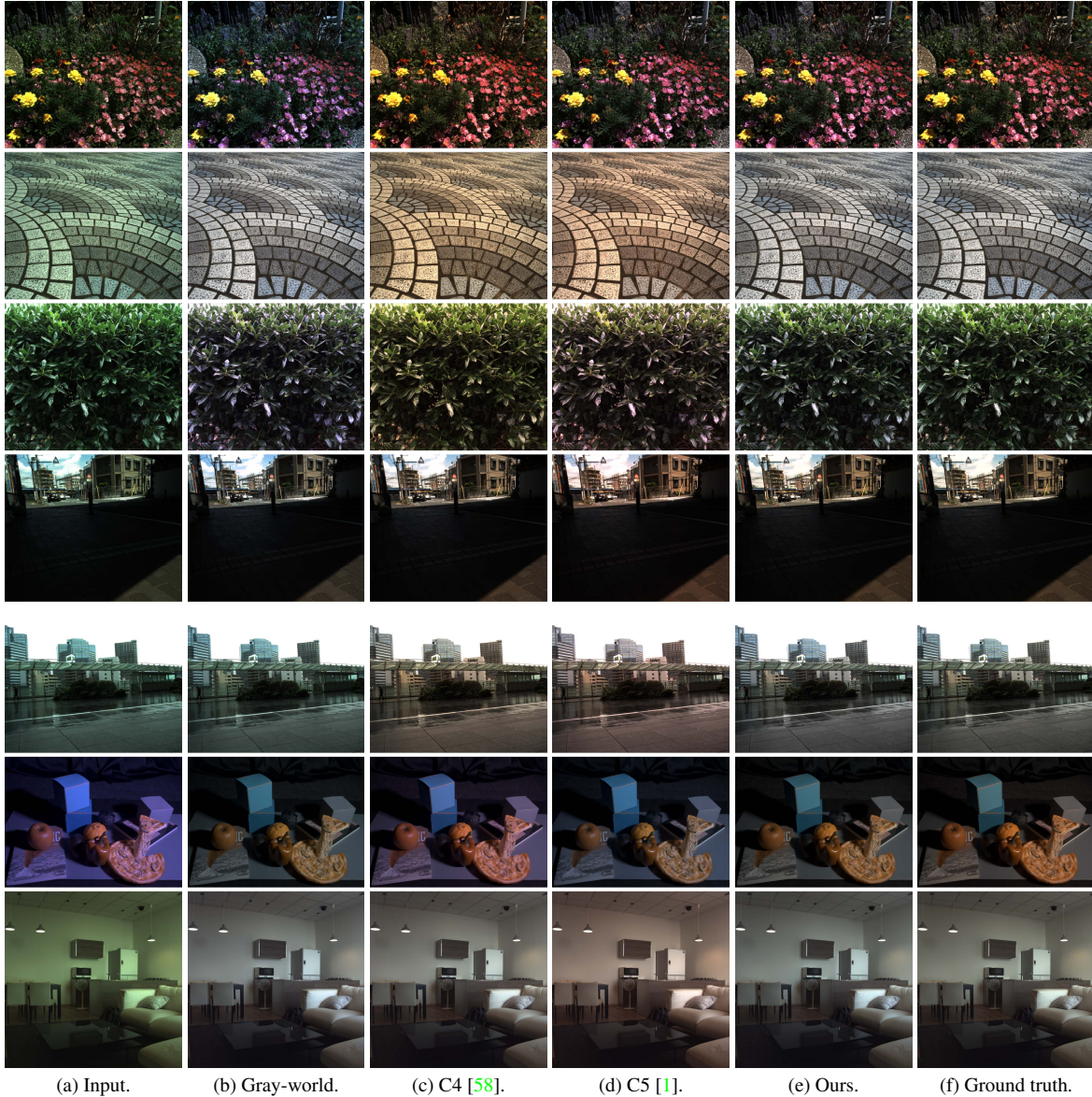
| (a) Input. | (b) Gray-world. | (c) C4 [58]. | (d) C5 [1]. | (e) Ours. | (f) Ground truth. |

Figure 7. Qualitative evaluations with Gray-world, C4 [58], and C5 [1].

| (a) DoLP. | (b) Ground truth. | (c) w/ Ach. | (d) w/o Ach. |

Figure 8. Failure case. (a) DoLP image. (b) Ground truth. (c) Our result using both achromatic and chromatic pixels. (d) Our result only using chromatic pixels.

tude is more affected by the diffuse reflectance r_d. Figure 9 shows two color charts captured under different illuminations. We linearly located the color chart, light source, and the camera to suppress specular reflection. In this case, the assumption disregarding the diffuse reflection incorrectly estimated the illumination colors (Fig. 9d). On the contrary, our method robustly predicted the illuminations (Fig. 9c). Our angular errors of these two scenes were 0.83 (top) and 1.13 (bottom), while those without considering diffuse reflection were 6.22 and 7.38, respectively. And for the 82 evaluation scenes, the mean angular error is 4.24 when disregarding the diffuse polarization.

Extension to multi-illumination scenes: Moreover, we aimed to handle scenes including several illuminations. Figure 10 shows three color charts illuminated by different il-

19746

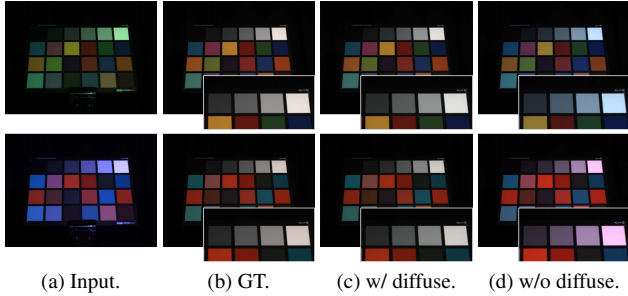(a) Input.   (b) GT.   (c) w/ diffuse.   (d) w/o diffuse.

Figure 9. The proposed method correctly handles the diffuse-dominated scenes. (a) Raw-RGB images. (b) White-balanced images using the ground-truth illuminations. (c) Our results. (d) White-balanced results without considering diffuse polarization.

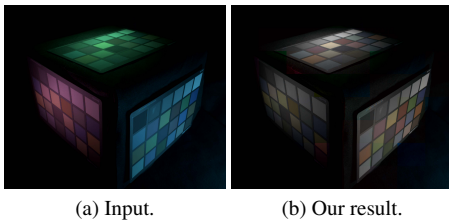(a) Input.   (b) Our result.

Figure 10. Our method manages the multi-illuminations. (a) Input images illuminated by three different illuminations. (b) Our results acquired by estimating the illumination colors on each image patch. All images are in sRGB color space.

lumination colors. Because our method can estimate illuminations almost pixel-wise, our result shown in Fig. 10b completely manages three different illuminations at the same time. We divided the images into 8×8 and separately computed the illuminations. For calculating the reliability, we used the same parameters described above. We also examined the outdoor scene shown in Fig. 11 including sunlit and shadow areas. Figure 11b shows the white-balanced result using only one illumination color computed by a color chart located in the sunlit area. In this image, we know that the shadow area is tinted with blue because this part is illuminated by the blue sky. However, our result (Fig. 11a) does not have this kind of unnatural effect. For this scene, we divided the image into 20×20 patches. Note that we estimated illuminations using the same scene without the color charts. For the discussion of the patch size, see supplementary materials.

6. Discussions

In this section, we explain several cases the introduced model Eq. (3) does not consider.

Directly observing minor light sources: Because our polarization model Eq. (3) assumes at least one reflection, directly observing minor light sources could harm the re-

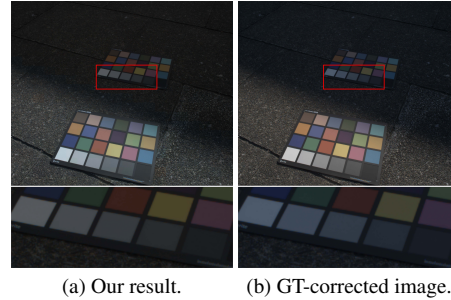(a) Our result.   (b) GT-corrected image.

Figure 11. Our method simultaneously estimates illuminations of shadow and sunlit pixels. (a) Our results acquired by estimating the illumination colors on each image patch. (b) White-balanced image using the ground-truth illumination from a sunlit color chart. All images are in sRGB color space.

sults. Scenes including blue skies are an example of this case because the contribution of the blue skies are quite minor than the sunlight. Even in these cases, we can estimate illumination colors by only using chromatic pixels (Fig. 8d), so proposing a novel algorithm is an issue for the future. Note that regarding major illuminations as achromatic does not degrade our results.

Special cases of multi-illuminations: Because Mueller matrices depend on the directions of incident light and view point, DoLP of achromatic pixels do not become achromatic when they are illuminated by several different illumination colors from different positions. Note that when these lights have the same color, the DoLP values of achromatic pixels become achromatic; thus, our method still works well.

RGB of incident Stokes vector is different: The model assumes the Stokes vector of the incident illumination is independent of wavelength, but multi-reflected light often violates this assumption. In this case, the estimated illuminations using chromatic pixels are heavily affected. However, since the pixels containing the multi-reflection do not contribute to the achromatic pixels, the effect of multi illumination is very limited.

7. Conclusion

In this paper, we proposed a new DoLP-based approach to solve the color constancy problem. We showed that the DoLP allows us to find achromatic pixels stably, and our experimental results demonstrate our state-of-the-art performance. Additionally, our method can estimate illuminations from chromatic pixels and handle multi-illumination scenes. Our method still has several limitations, and a more detail runtime investigation will be needed. However, this paper conclusively proved the impressive contribution of DoLP to the color constancy problem.

References

[1] Mahmoud Afifi, Jonathan Barron, Chloe LeGendre, Yun-Ta Tsai, and Francois Bleibel. Cross-camera convolutional color constancy. In *Int. Conf. Comput. Vis.*, pages 1981–1990, 2021. 2, 6, 7

[2] Mahmoud Afifi and Michael Brown. What else can fool deep learning? Addressing color constancy errors on deep neural network performance. In *Conf. Comput. Vis. Pattern Recog.*, pages 243–252, 2019. 1

[3] Vivek Agarwal, Andrei Gribok, and Mongi Abidi. Machine learning approach to color constancy. *Neural Netw.*, 20:559–563, 07 2007. 2

[4] Vivek Agarwal, Andrei Gribok, Andreas Koschan, and Mongi Abidi. Estimating illumination chromaticity via kernel regression. In *Int. Conf. Image Process.*, pages 981–984, 2006. 2

[5] Alexander Andreopoulos and John Tsotsos. On sensor bias in experimental methods for comparing interest-point, saliency, and recognition algorithms. *Trans. Pattern Anal. Mach. Intell.*, 34(1):110–126, 2012. 1

[6] Lawrence Arend, Adam Reeves, James Schirillo, and Robert Goldstein. Simultaneous color constancy: Papers with diverse Munsell values. *J. Opt. Soc. Am. A*, 8(4):661–672, Apr 1991. 1

[7] Gary Atkinson and Edwin Hancock. Multi-view surface reconstruction using polarization. *Int. Conf. Comput. Vis.*, 1:309–316, 2005. 2

[8] Gary Atkinson and Edwin Hancock. Polarization-based surface reconstruction via patch matching. In *Conf. Comput. Vis. Pattern Recog.*, volume 1, pages 495–502, June 2006. 3

[9] Seung-Hwan Baek, Daniel Jeon, Xin Tong, and Min Kim. Simultaneous acquisition of polarimetric SVBRDF and normals. *ACM Trans. Graph.*, 37(6), Dec. 2018. 2, 3

[10] Jonathan Barron. Convolutional color constancy. *Int. Conf. Comput. Vis.*, pages 379–387, 2015. 2

[11] Jonathan Barron and Yun-Ta Tsai. Fast Fourier color constancy. In *Conf. Comput. Vis. Pattern Recog.*, pages 6950–6958, 2017. 1, 2, 6

[12] Gershon Buchsbaum. A spatial processor model for object colour perception. *J. Franklin Inst.*, 310(1):1–26, 1980. 1, 2, 6

[13] Homer Chen, Chun-Hung Shen, and Pei-Shan Tsai. Edge-based automatic white balancing with linear illuminant constraint. In *Vis. Commun. Image Process.*, volume 6508, pages 484–495, 2007. 2

[14] Dongliang Cheng, Dilip Prasad, and Michael Brown. Illuminant estimation for color constancy: Why spatial-domain methods work and the role of the color distribution. *J. Opt. Soc. Am. A*, 31(5):1049–1058, May 2014. 6

[15] Zhaopeng Cui, Jinwei Gu, Boxin Shi, Ping Tan, and Jan Kautz. Polarimetric multi-view stereo. In *Conf. Comput. Vis. Pattern Recog.*, pages 369–378, July 2017. 3

[16] Marc Ebner. Color constancy based on local space average color. *Mach. Vis. Appl.*, 20:283–301, 07 2009. 2

[17] Graham Finlayson and Elisabetta Trezzi. Shades of gray and colour constancy. In *Color Imag. Conf.*, pages 37–41, 2004. 1, 2, 6

[18] Gregor Fischer, Karin Kolbe, and Matthias Sajjaa. WhitebalPR: automatic white balance by polarized reflections. In Jeffrey M. DiCarlo and Brian G. Rodricks, editors, *Digital Photography IV*, volume 6817, pages 115 – 125. International Society for Optics and Photonics, SPIE, 2008. 2

[19] Brian Funt and Lilong Shi. The effect of exposure on maxRGB color constancy. In *SPIE Int. Soc. for Opt. Eng.*, volume 7527, page 75270, 02 2010. 2

[20] Brian Funt and Lilong Shi. The rehabilitation of maxRGB. In *Color Imag. Conf.*, pages 256–259, 2010. 1, 2

[21] Brian Funt and Weihua Xiong. Estimating illumination chromaticity via support vector regression. In *J. Image. Sci. Tech.*, volume 50, pages 47–52, 2004. 1, 2

[22] Peter Vincent Gehler, Carsten Rother, Andrew Blake, Tom Minka, and Toby Sharp. Bayesian color constancy revisited. In *Conf. Comput. Vis. Pattern Recog.*, pages 1–8, 2008. 5, 6

[23] Theo Gevers. and Arnold Smeulders. PicToSeek: combining color and shape invariant features for image retrieval. *Trans. Image Process.*, 9(1):102–119, 2000. 1

[24] Arjan Gijsenij, Partha Das, and Anil Baslamisli. Color constancy: research website on illuminant estimation. http://colorconstancy.com/index.html, Oct 2011. (Accessed on 05/11/2021). 6

[25] Arjan Gijsenij and Theo Gevers. Color constancy by local averaging. In *Int. Conf. of Image Anal. and Process. - Workshops*, pages 171–174, 10 2007. 2

[26] Arjan Gijsenij, Theo Gevers, and Joost van de Weijer. Physics-based edge evaluation for improved color constancy. In *Conf. Comput. Vis. Pattern Recog.*, pages 581–588, 2009. 2

[27] Arjan Gijsenij, Theo Gevers, and Joost van de Weijer. Improving color constancy by photometric edge weighting. *Trans. Pattern Anal. Mach. Intell.*, 34(5):918–929, 2012. 6

[28] Glenn Healey. Estimating spectral reflectance using highlights. *Image Vis. Comput.*, 9(5):333–337, 1991. 2

[29] Daniel Hernandez-Juarez, Sarah Parisot, Benjamin Busam, Ales Leonardis, Gregory Slabaugh, and Steven McDonagh. A multi-hypothesis approach to color constancy. In *Conf. Comput. Vis. Pattern Recog.*, pages 2267–2277, 2020. 2

[30] Yuanming Hu, Baoyuan Wang, and Stephen Lin. FC 4: fully convolutional color constancy with confidence-weighted pooling. In *Conf. Comput. Vis. Pattern Recog.*, pages 4085–4094, 2017. 1, 2, 6

[31] Hamid Reza Vaezi Joze and Mark Drew. Exemplar-based color constancy and multiple illumination. *Trans. Pattern Anal. Mach. Intell.*, 36(05):860–873, 2014. 1

[32] Achuta Kadambi, Vage Taamazyan, Boxin Shi, and Ramesh Raskar. Polarized 3D: high-quality depth sensing with polarization cues. In *Int. Conf. Comput. Vis.*, pages 3370–3378, Dec 2015. 3

[33] Yuhi Kondo, Taishi Ono, Legong Sun, Yasutaka Hirasawa, and Jun Murayama. Accurate polarimetric BRDF for real polarization scene rendering. In *Eur. Conf. Comput. Vis.*, pages 220–236, 11 2020. 2, 3

[34] Teppei Kurita, Shun Kaizu, Yuhi Kondo, Yasutaka Hirasawa, and Ying Lu. Image processing device and image processing method. U.S. Patent 10,460,422, issued Oct. 29, 2019. 5

[35] Edwin Land. The retinex theory of color vision. *Sci. Amer.*, 237(6):108–129, 1977. 1, 2, 6

[36] Chenyang Lei, Xuhua Huang, Mengdi Zhang, Qiong Yan, Wenxiu Sun, and Qifeng Chen. Polarized reflection removal with perfect alignment in the wild. In *Conf. Comput. Vis. Pattern Recog.*, June 2020. 2

[37] Bing Li, De Xu, Weihua Xiong, and Songhe Feng. Color constancy using achromatic surface. *Color Res. Appl.*, 35(4):304–312, 2010. 2

[38] Rui Li, Simeng Qiu, Guangming Zang, and Wolfgang Heidrich. Reflection separation via multi-bounce polarization state tracing. In *Eur. Conf. Comput. Vis.*, pages 781–796. Springer, 2020. 2

[39] Yi-Chen Lo, Chia-Che Chang, Hsuan-Chao Chiu, Yu-Hao Huang, Chia-Ping Chen, Yu-Lin Chang, and Kevin Jou. CLCC: Contrastive learning for color constancy. In *Conf. Comput. Vis. Pattern Recog.*, pages 8053–8063, 2021. 2

[40] Youwei Lyu, Zhaopeng Cui, Si Li, Marc Pollefeys, and Boxin Shi. Reflection separation using a pair of unpolarized and polarized images. In *Adv. Neural Inf. Process. Sys,*, volume 32, 2019. 2

[41] Yanlin Qian, Ke Chen, Jarno Nikkanen, Joni-Kristian Kämäräinen, and Jiri Matas. Recurrent color constancy. In *Int. Conf. Comput. Vis.*, pages 5459–5467, 2017. 1, 2

[42] Yanlin Qian, Joni-Kristian Kämäräinen, Jarno Nikkanen, and Jiri Matas. On finding gray pixels. In *Conf. Comput. Vis. Pattern Recog.*, pages 8054–8062, 2019. 2, 6

[43] Stefan Rahmann. Polarization images: A geometric interpretation for shape analysis. In *Int. Conf. Pattern Recog.*, volume 3, pages 538–542, 2000. 2

[44] Stefan Rahmann and Nikos Canterakis. Reconstruction of specular surfaces using polarization imaging. In *Conf. Comput. Vis. Pattern Recog.*, volume 1, pages I–I, 2001. 2

[45] Matthias Sajjaa and Gregor Fischer. Automatic white balance: WhitebalPR using the dichromatic reflection model. In *Soc. Photo-Op. Inst. Eng. Conf. Series*, volume 7250, page 72500D, 2009. 2

[46] Steven Shafer. Using color to separate reflection components. *Color Research & Application*, 10(4):210–218, 1985. 3

[47] Wu Shi, Chen Change Loyand, and Xiaoou Tang. Deep specialized network for illuminant estimation. In *Eur. Conf. Comput. Vis.*, pages 371–387, 2016. 1, 2

[48] William Smith, Ravi Ramamoorthi, and Silvia Tozza. Linear depth estimation from an uncalibrated, monocular polarisation image. In *Eur. Conf. Comput. Vis.*, pages 109–125, 2016. 2, 3

[49] Robby Tan, Ko Nishino, and Katsushi Ikeuchi. Color constancy through inverse-intensity chromaticity space. *J. Opt. Soc. Am. A*, 21(3):321–334, Mar 2004. 2

[50] Shoji Tominaga and Brian Wandell. Standard surface-reflectance model and illuminant estimation. *J. Opt. Soc. Amer. A*, 6(4):576–584, 05 1989. 2

[51] Joost van de Weijer, Theo Gevers, and Arjan Gijsenij. Edge-based color constancy. *Trans. Image Process.*, 16(9):2207–2214, 2007. 1, 2, 6

[52] Ning Wang, De Xu, and Bing Li. Edge-based color constancy via support vector regression. *IEICE Trans. Inf. Sys.*, E92.D(11):2279–2282, 2009. 2

[53] Lawrence Wolff and Terrance Boult. Constraining object features using a polarization reflectance model. *Trans. Pattern Anal. Mach. Intell.*, 13(7):635–657, July 1991. 2

[54] Jin Xiao, Shuhang Gu, and Lei Zhang. Multi-domain learning for accurate and few-shot color constancy. In *Conf. Comput. Vis. Pattern Recog.*, pages 3255–3264, 2020. 2

[55] Weihua Xiong, Brian Funt, Lilong Shi, Sung-Su Kim, Byoung-Ho Kang, Seongdeok Lee, and Chang Yeong Kim. Automatic white balancing via gray surface identification. In *Color Imag. Conf.*, pages 143–146, 11 2007. 2

[56] Tomohiro Yamazaki, Yasushi Maruyama, Yusuke Uesaka, Motoaki Nakamura, Yoshihisa Matoba, Takashi Terada, Kenta Komori, Yoshiyuki Ohba, Shinichi Arakawa, Yasutaka Hirasawa, Yuhi Kondo, Jun Murayama, Kentaro Akiyama, Yusuke Oike, Shuzo Sato, and Takayuki Ezaki. Four-directional pixel-wise polarization CMOS image sensor using air-gap wire grid on 2.5-μm back-illuminated pixels. In *Int. Elec. Devices Meeting (IEDM)*, pages 8.7.1–8.7.4, 2016. 2

[57] Jie Yang, Rainer Stiefelhagen, Uwe Meier, and Alex Waibel. Visual tracking for multimodal human computer interaction. In *SIGCHI Conf. Human Factors Comput. Syst.*, pages 140–147, 1998. 1

[58] Huanglin Yu, Ke Chen, Kaiqi Wang, Yanlin Qian, Zhaoxiang Zhang, and Kui Jia. Cascading convolutional color constancy. In *Conf. on Artif. Intell.*, pages 12725–12732, 2020. 2, 6, 7